JOURNAL OF AEROSOL MEDICINE AND PULMONARY DRUG DELIVERY
Volume 27, Number 0, 2014

Pp. 1–9
DOI: 10.1089/jamp.2013.1093

Measurements of Droplet Size Distribution and Analysis of Nasal Spray Atomization from Different Actuation Pressure

Kiao Inthavong, PhD,[1] Man Chiu Fung, PhD,[1] William Yang, PhD,[2] and Jiyuan Tu, PhD[1]

Abstract

Background: To evaluate the deposition efficiency of spray droplets in a nasal cavity produced from a spray device, it is important to determine droplet size distribution, velocity, and its dispersion during atomization. Due to the limiting geometric dimensions of the nasal cavity airway, the spray plume cannot develop to its full size inside the nasal vestibule to penetrate the nasal valve region for effective drug deposition.
Methods: Particle/droplet image analysis was used to determine local mean droplet sizes at eight regions within the spray plume under different actuation pressures that represent typical hand operation from pediatric to adult patients.
Results: The results showed that higher actuation pressure produces smaller droplets in the atomization. Stronger actuation pressure typical of adult users produces a longer period of the fully atomized spray stage, despite a shorter overall spray duration. This produces finer droplets when compared with the data obtained by weaker actuation pressure, typical of pediatric users.
Conclusion: The experimental technique presented is able to capture a more complete representation of the droplet size distribution and the atomization process during an actuation. The measured droplet size distribution produced can be related to the empirically defined deposition efficiency curve of the nasal cavity, allowing a prediction of the likely deposition.

Key words: nasal drug delivery, automated actuation, spray pattern, particle/droplet image analysis, spray atomization

Introduction

NASAL SPRAY DRUG DELIVERY is widely used in the pharmaceutical industry and has enormous potential to deliver new systemic drugs to the human body via the nasal cavity.[1] The drug delivery performance of a nasal spray device depends on many factors, such as the design of the pump, the shape of the orifice, physical properties of the formulation, and patient handling.[2–4] Nevertheless, deposition rates and patterns of the atomized droplets indicate the spray device performance within the nasal cavity. Suman *et al.*[5] suggested that research is needed to define the impact of spray pump characteristics on deposition pattern and drug response.

Deposition of micrometer-sized aerosols in the nasal cavity is primarily driven by inertial impaction[6] defined through the so-called inertial parameter[2,7] (or the particle Stokes number[8]), which is proportional to the inhalation flow rate Q and the square of the aerosol aerodynamic diameter d^2. However, these parameters are mainly valid when the droplet is entrained in the fluid, and do not consider initial droplet conditions that exhibit high slip velocities that void the validity of the inertial parameter.

The influence of the initial droplet velocity and its oriented direction created by spray atomization has been visualized computationally.[9,10] The results showed that particles of $>50\,\mu$m impacted onto the roof of the nasal vestibule because of its high inertial property. The initial swirling behavior of the atomized droplets is produced through the pressure-swirl atomizer itself. This helps to reduce the droplet velocity before the droplets become entrained in the inhaled air. Foo *et al.*[11] suggested that the spray cone angle and administration angle are critical factors for deposition efficiency, as not all spray droplets

[1]School of Aerospace, Mechanical and Manufacturing Engineering, RMIT University, Bundoora, Victoria, Australia.
[2]CSIRO Process Science and Engineering, Clayton South, Victoria, Australia.

delivered by a nasal spray pump can enter the main nasal passage. Experimental visualization[2] and *in vivo* deposition studies[12,13] also showed that high deposition occurred in the anterior nasal cavity because of the inertial deposition of droplets. Consequently, the fraction of droplets that penetrate the nasal valve region is low, leading to low drug utilization.

Ongoing investigations aimed at improving the nasal drug deposition efficiency have determined that if spray velocity and droplet size are decreased, nasal sprays can cover more area and may penetrate the nose beyond the nasal valve region.[14] Such means may be achieved through manipulation of the internal atomizer of the spray device to produce a desirable atomization of the liquid drug formulation into droplets of sufficiently small size and low velocity. Therefore, studying the atomization process is paramount for understanding and predicting spray performance, because it dictates the droplet formation and initial velocities as it enters the nasal cavity.

A number of studies have quantified the outcomes of the spray atomization but do not actually discuss the physical behavior of spray development. For example, Mitchell *et al.*,[15] Dayal *et al.*,[4] Guo and Doub,[16] Guo *et al.*,[17] and Liu *et al.*[18] all used laser diffraction to characterize the aerosol velocity and droplet size distribution of nasal spray pumps, and found that stroke length and actuation velocity had an impact on droplet size distribution and spray plume geometry. Kippax *et al.*[19] and Doughty *et al.*[20] also used phase Doppler anemometry (PDA), but related the time-varying droplet size distribution to the force of actuation with human manual actuation.

Laser diffraction techniques using PDA measurements are limited to a single point location, at a distance from the pump orifice. In the work by Liu *et al.*,[18] 13 sample positions in a horizontal cross section were taken at a distance of 3 cm from the pump orifice. Using an alternate method, Inthavong *et al.*[21] used particle image velocimetry and particle/droplet image analysis (PDIA) to study the external spray characteristics and its droplet size distribution from a continuous spray from a nonactuating nasal spray device. Later Fung *et al.*[22] investigated the external characteristics of a spray with different actuation force, mimicking the hand operation of adult and pediatric patients by using an in-house automated test station. However, the droplet size distribution was not quantified.

By using PDIA and high-speed filming, this study extends the work of Kippax *et al.*[19] and Doughty *et al.*[20] by investigating the influence of actuation force on the atomization process and its subsequent droplet size distribution and velocity. By using high-speed filming, the external spray characteristics and spray actuation can be visualized, and the PDIA system is used to determine the droplet size distribution and its velocity within a region rather than a point location. The application of the measured data is shown through a computational fluid dynamics (CFD) simulation of droplets introduced into a realistic human nasal cavity.

Materials and Methods

Automated mechanical actuation system

An in-house automated actuation system was developed, shown in Figure 1, which uses a pneumatic actuator with a two-way solenoid valve controlled by a programmable logic control unit. The spray bottle is a commercially available over-the-counter nasal spray device kindly provided by GlaxoSmithKline, capable of delivering 200 sprays per bottle with 50 μg of formulation per actuation during normal operation. A large water tank (20 L) filled with distilled water was attached to the nasal spray bottle to ensure a consistent water level in the nasal spray bottle and constant internal pressure. The spray bottle was fixed at the base on the actuator to avoid undesired lateral motion during actuation. Pressure was supplied by the pressure mains and adjustable by a pressure regulator. In the experiment, three actuation pressures were applied (2.05, 2.45, and 2.65 bar), which are within the range of hand operation by pediatric to adult patients.[22] The system was placed on a transverse unit, so it can be maneuvered with high precision (± 17 μm) to any desired location.

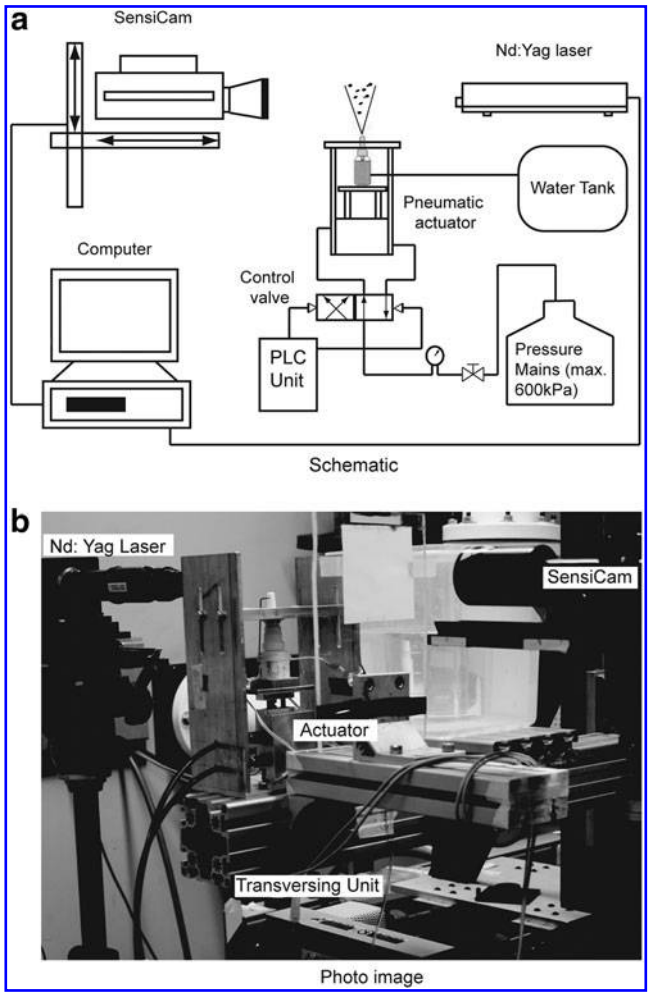

FIG. 1. **(a)** Schematic and **(b)** photo image of the experimental setup for PDIA and high-speed filming of spray atomization from nasal spray device.

The timing signal generated by the programmable logic control unit sends a simple on/off pattern to push the pneumatic actuator up and down. The actuator then retracts back to its rest position after completing a full actuation. The time between each actuation was set to 2.2 sec to allow sufficient settling time of residual airborne droplets to disappear before the next actuation cycle. The spray bottle was

initially held at rest for 2.2 sec, and then a signal pulse (synchronized to a computer and the PDIA system) was used to activate the actuator.

PDIA

The PDIA light source was a New Wave 120 mJ double-pulsed Nd:YAG laser, connected with a SensiCam 12-bit digital charge-coupled device camera (resolution of 1,280 × 1,024 pixels). The spray droplet images were captured with a long-distance microscope lens with a magnification of 2.23. The physical size of the field-of-view (FOV) was 3.85 mm × 3.08 mm with resolution of 3.01 μm/pixel. This meant that to capture the spray plume in the near-nozzle region, 11 FOV regions are required (Fig. 2). These regions are made up of four rows, labeled R1 to R4, covering a height of 12.32 mm from the spray device. Each column is labeled C1 to C5 moving from left to right.

For each image, the PDIA system detects individual droplets and its diameter by an automated segmentation threshold algorithm located on the focal plane.[23,24] Droplet diameters were estimated by the pixel area covered by the droplet with a correction for out-of-focus effect. This correction algorithm is based on the ratio of the dark core droplet area and its grayed out-of-focus border area. A relationship between this ratio and the focal distance is used in the calibration file of the visualization system, to calculate the true droplet diameter. To achieve a sufficient statistical average, a set of 100 image pairs for each FOV at different actuation times were obtained. Further details of the image processing and droplet analysis have been reported previously by the authors.[21]

Results and Discussion

Nozzle displacement and spray development

By using high-speed filming, the nozzle displacement during spray actuation for three different pressure cases was determined (Fig. 3). After preliminary testing, up to six sets of filming per case were performed and the results averaged; any measurements experiencing timing errors were discarded. The profile for the 2.45 bar case corresponds well with the physical behavior of spray actuation. There is an initially rapid increase in the displacement as the actuator moves up to engage the spring. A momentary pause in the displacement occurs as the actuation force has to overcome the spring resistance (see Fig. 3d) and also the fluid surface tension as it exits the orifice. This is followed by a steady increase in the displacement before flattening after complete actuation. Similar profiles are produced by the other cases. For the lower 2.05 bar case, the lack of force extends the actuation duration, because it takes longer to overcome the same amount of resistance. Conversely, the higher 2.65 bar case exhibits a much faster actuation time. Instantaneous times labeled as S1, S2, and S3 on the graphs are selected for repeated PDIA imaging of the spray for the droplet size analysis. This means that we can observe any temporal variation in the droplet size and velocity during actuation by comparisons of the set of images taken at S1, S2, and S3.

The spray cone development in the near-nozzle region (< 3 mm from the spray exit) during atomization is shown in Figure 4. Three stages were identified where the spray was (i) expanding, (ii) fully developed, or (iii) collapsing. During the expanding period, the liquid forms a so-called *distorted pencil* shape,[22] before it is elongated and is far enough from the nozzle to allow instabilities on the liquid sheet to resonate and atomize. After this, the spray reaches its maximum cone angle and mass flow rate as it becomes fully developed and the atomization becomes constant. As spray actuation is completed, the pressure required to squeeze the fluid through the orifice diminishes, causing the spray cone to collapse in on itself, forming a water column. A high-speed film of this spray formation can be found online at www.youtube.com/watch?v = _xid3FguMHE. The

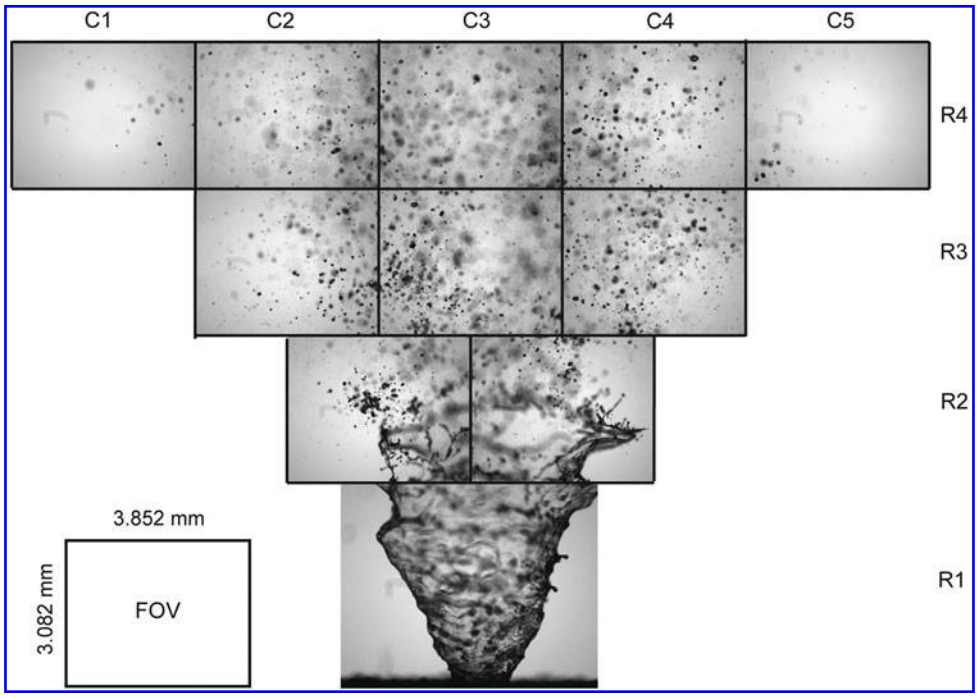

FIG. 2. A collation of single-shot images at 11 different FOV regions of the spray plume near the nozzle/orifice. The letter R represents the rows, and C represents the columns defined by each FOV.

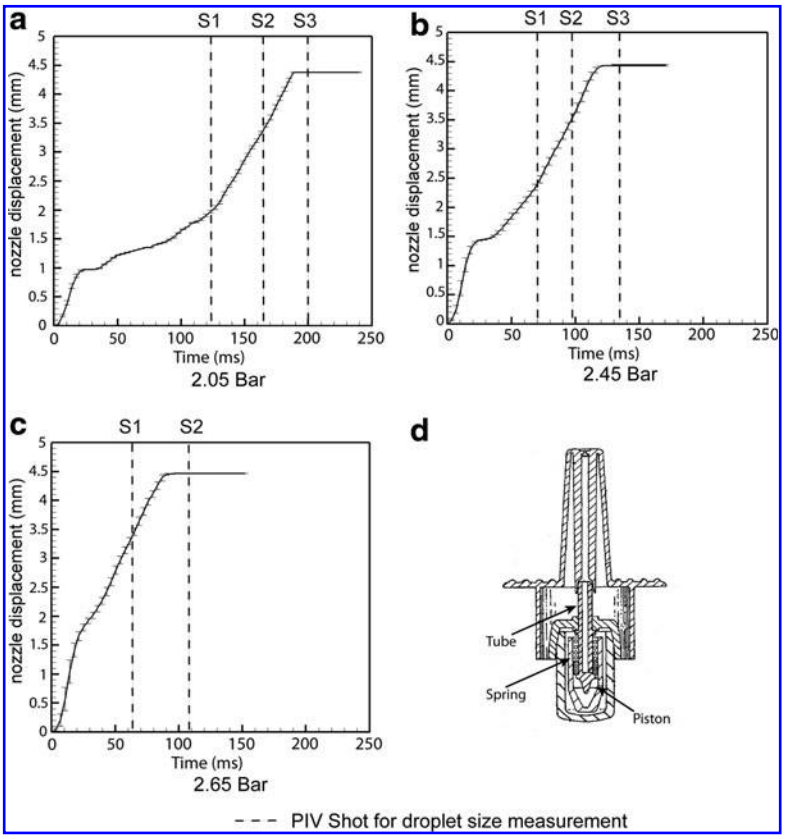

FIG. 3. Nozzle displacement history for **(a)** 2.05 bar, **(b)** 2.45 bar, and **(c)** 2.65 bar actuation pressure and **(d)** schematic of internal spray atomizer.

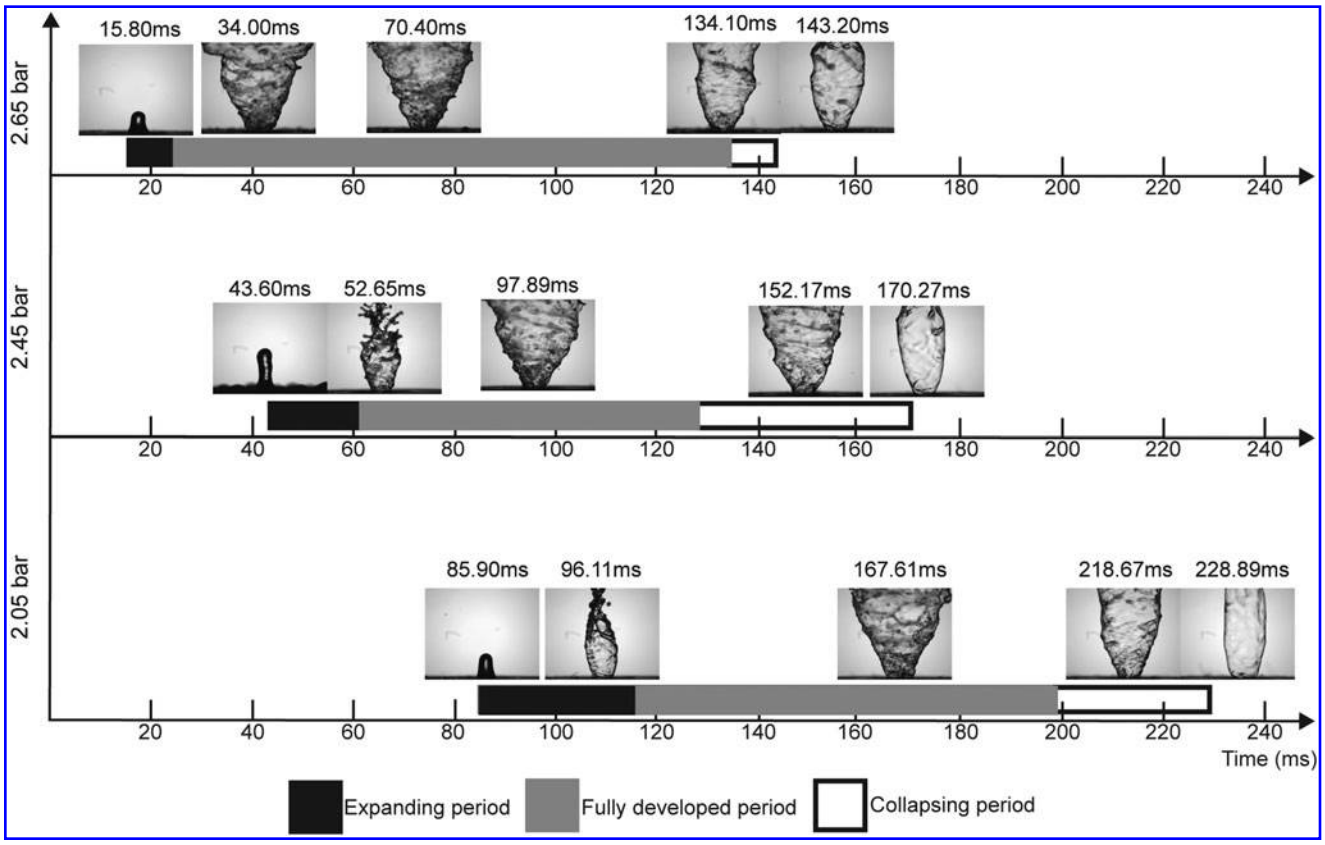

FIG. 4. Spray plume development as a function of time where $t = 0$ sec represents the start of actuation. It can be seen that the higher actuation pressure produces faster and shorter atomization. Three periods, *i.e.*, expanding, fully developed, and collapsing, are defined based on the shape of the spray plume.

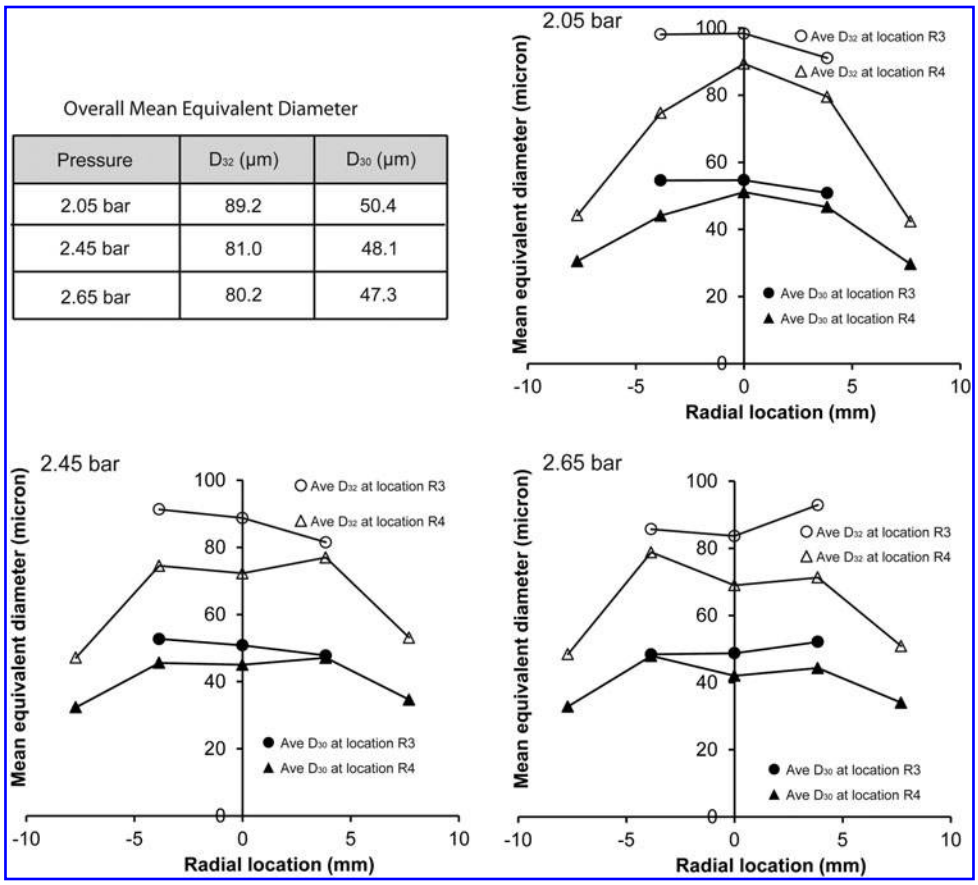

FIG. 5. The overall mean equivalent diameters defined through the Sauter mean (D_{32}) and volume mean (D_{30}) diameters in the near-nozzle FOV regions along rows R3 and R4 of the spray plume under different actuation pressures: 2.05 bar, 2.45 bar, and 2.65 bar.

expansion period of the 2.65 bar case is the fastest while its fully developed period occupies most of the spraying time, which produces smaller droplet sizes during atomization.[25] The fully atomized period produces the most consistent spray characteristic, finer droplets, and a complete spray cone angle. An increase in actuation effort increases the duration of the fully developed period, implying that greater atomization occurs and more droplets are produced.

Droplet size analysis

The averaged droplet diameter was determined for the three different pressure cases at each FOV region along rows R3 and R4 defined in Figure 2 (eight regions in total). For each FOV region, a set of 100 image pairs were captured at two or three time instances (based on the pressure case), during the developed atomization stage where the spray plume was relatively full. The time instances are shown earlier in Figure 3, labeled as S1, S2, and S3, and a total of 200 images per time instance were acquired. Two equivalent diameters, D_{32} (Sauter mean diameter) and D_{30} (volume mean diameter), were used to describe the droplet size and its variation across the spray plume.

The Sauter mean diameter, D_{32}, represents the mean diameter of a spherical droplet having the same volume-to-surface area ratio and is relevant to drug delivery, because the surface area produces greater reactions for drug penetration through the respiratory mucus. Figure 5 shows that the 2.65 bar case produced the smallest equivalent diameters (both D_{30} and D_{32}), and the 2.05 bar case produced the largest equivalent diameters due to the lower actuation force. The D_{32} shows similar trends to the D_{30}, but comparatively the diameters differ the greatest in the center and are more similar at the periphery of the spray. As D_{32} is a volume-to-surface area ratio, the results suggest that the droplets are more spherical in the center and more distorted at the edges. This may be attributed to the droplets undergoing secondary atomization.

TABLE 1. COMPARISON OF CUMULATIVE VOLUME MEAN DIAMETER (D_V)

	Suman et al. *(2002)*[3]	*Dayal* et al. *(2004)*[4]	*Liu* et al. *(2010)*[18]	*Current study*	
				2.05 bar	*2.65 bar*
D_{v10}	21.5	23–40		40	34
D_{v50}	41–43	42–86	31–42	110	103
D_{v90}	77–87	72–160		258	240
Distance from nozzle (mm)	45	30	30	6–12	6–12

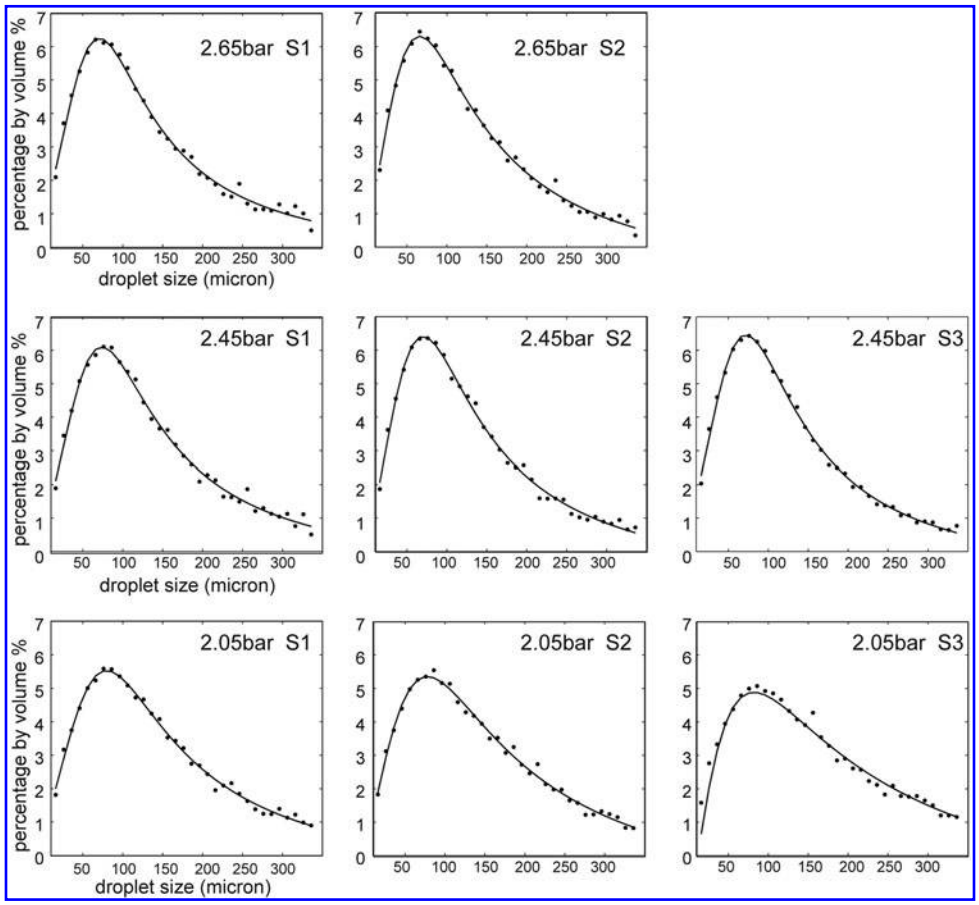

FIG. 6. Averaged droplet size distribution across rows R3 and R4. Temporal variation of the overall mean equivalent diameters are defined through the Sauter mean (D_{32}) and volume mean (D_{30}) diameters in the near-nozzle FOV regions along rows R3 and R4 of the spray plume under different actuation pressures: 2.05 bar, 2.45 bar, and 2.65 bar.

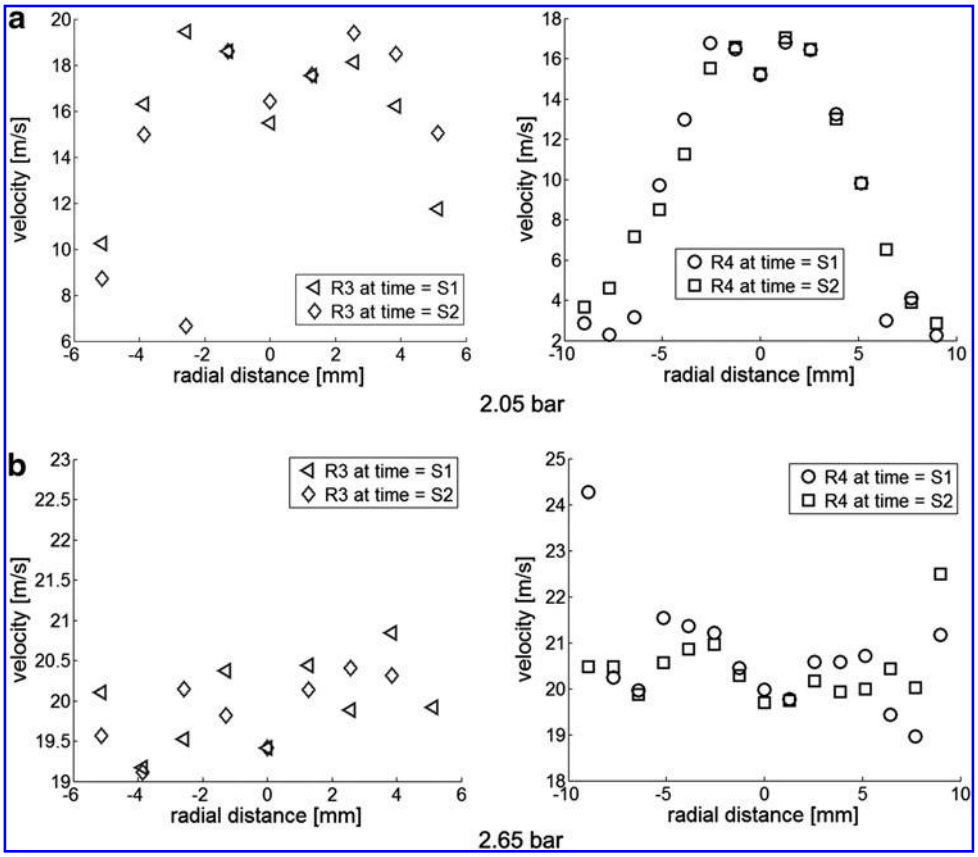

FIG. 7. Averaged droplet velocity across the rows R3 and R4, taken at **(a)** 2.05 bar for $t_1 = 126$ msec and $t_2 = 168$ msec and **(b)** 2.65 bar for $t_1 = 88$ msec and $t_2 = 134$ msec after liquid has exited from the nozzle.

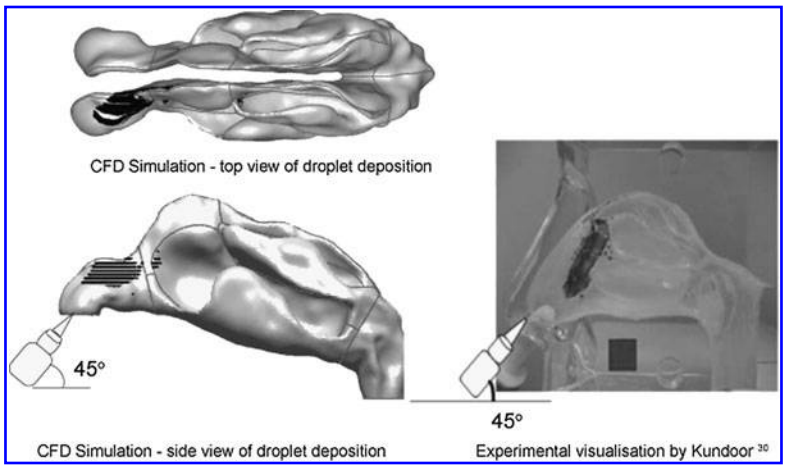

FIG. 8. Droplet deposition pattern using CFD simulations, and its comparison with experimental visualization from Kundoor and Dalby.[30]

The efficiency and absorption rate of a drug are proportional to the surface area. An increase in the droplet diameter produces a surface area to a squared power ($A = \pi d^2$), *i.e.*, the surface area increases at a much faster rate for a given increase in diameter. Therefore, for a given mass, finer droplets produce a larger total contact surface area, because the number of droplets is greater.

According to Fung *et al.*,[26] fine droplets are transported and dispersed throughout the spray from the presence of turbulent eddies in the flow. These droplets quickly lose their momentum and become entrained in the flow field. As a result, the particles then possess longer residence time than the large droplets, and accumulate close to the nozzle region. A further cause of larger droplets for row R3 is its proximity to the breakup length, where the liquid ligaments from atomization begin to break off into droplets. For each row, the far radial locations exhibit smaller droplets, which are caused by the spray droplets undergoing secondary breakup.

An additional analysis was performed to obtain the averaged D_{30} droplet size in the FOV regions R4C2, R4C3, and R4C4. This excludes the two far radial FOVs R4C1 and R4C5, given that these two locations are unlikely to be reproduced inside the narrow nasal cavity.[27] This gives D_{30} values of 47.3 μm, 48.2 μm, and 50.4 μm for the pressure cases 2.05 bar, 2.45 bar, and 2.65 bar. Comparisons with existing data in the literature were performed and are summarized in Table 1, which compares the cumulative volume mean diameter of the spray. In the current study, the 2.05 bar and 2.65 bar cases are chosen for comparison. The droplet size of the current study is much larger than those reported in the literature, and this is due to two reasons. Firstly, Suman *et al.*,[3] Dayal *et al.*,[4] and Liu *et al.*[18] applied the laser diffraction technique to measure the spray droplet size at a single point, whereas PDIA measures the diameter of spray droplet in a two-dimensional 3.852 mm × 3.082 mm region. Secondly, the location of the measurement point from the literature is farther downstream, where secondary breakup occurs, leading to finer droplets—a phenomenon verified by Dayal *et al.*[4]

The temporal variation for the averaged droplet size distribution at different instantaneous moments, S1, S2, and S3, during atomization is given in Figure 6. All droplet size distributions exhibit a single modal profile biased to the smaller droplet size. Differences in the distribution profiles between each instantaneous moment are more noticeable for the 2.05 bar case, where the droplets occurring later in the atomization (t = S3) exhibit a flatter single modal profile. The profiles occurring at S1 and S2 for the 2.65 bar case are very similar. This supports the earlier observations that a higher pressure produces a consistent spray characteristic during the fully developed period (Fig. 4). The profiles also serve as quantitative data that can be used for setting realistic initial boundary conditions for nasal spray drug delivery droplet size distributions in CFD simulations. Each profile can be curve-fitted to the following equation:

$$f(x) = (a_1x^2 + a_2x + a_3)/(x^2 + a_4x + a_5)$$

where the coefficients a can be determined by a curve fit. As an example, for the 2.65 bar case taken at time S1, the coefficients are $a_1 = 0.00733$, $a_2 = 4.43$, $a_3 = 54.13$, $a_4 = -86.4$, and $a_5 = 6{,}397$.

Atomized droplet velocities

The averaged local droplet velocity for each FOV along rows R3 and R4 is shown in Figure 7. For the 2.05 bar case, a parabolic velocity profile is found with peak velocities occurring in the middle regions of the spray, whereas at the spray periphery, low velocities occur. In contrast, the velocity profile remains relatively constant around 21 m/sec across the width of the spray, for an actuation pressure of 2.65 bar. There is little variation between all profiles at the two atomization times within the fully atomized period.

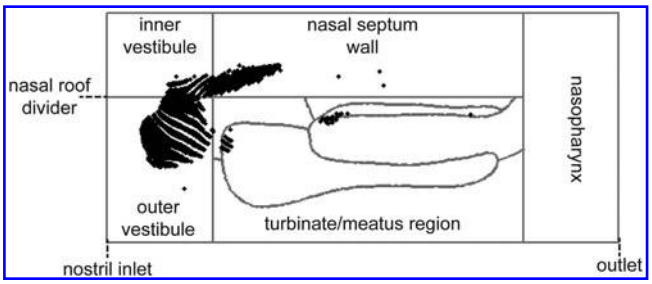

FIG. 9. Droplet deposition in the left nasal chamber using the initial droplet conditions produced from the spray experiments in the 2.65 bar case. The deposition pattern is displayed in the *uv*-plane.

Given the high velocities and large droplet formation near the nozzle from hand-actuated spray pumps, new device designs are needed to overcome these barriers to reduce droplet deposition by inertial impaction in the anterior nasal cavity. The reduction of droplet inertia is most sensitive to droplet diameter, because the inertia is proportional to the square of droplet size. This reduction enhances the ability for droplets to trace or follow the airflow streamlines more readily, enhancing the transport through the nasal valve. However, if the droplets follow the airflow too faithfully, then the droplets may exit the nasal cavity completely.

Drug delivery deposition prediction

Deposition studies of particles in the nasal cavity have been reported experimentally by many researchers.[2,6,10,28,29] Using the same techniques and a validated computational model,[10,31] we present an application of the current results serving as initial boundary conditions for CFD simulations to predict drug delivery deposition in the nasal cavity. The initial droplet size distribution and its velocity were taken from the 2.65 bar case during the fully atomized region where the spray characteristics are consistent. The total inhalation rate at the nasopharynx exit was set to 10 L/min, representing light inhaled effort, and the insertion angle is 45°.

The deposition in Figure 8 shows local concentration of droplets in the upper vestibule that is in line with the 45° orientation, similar to the experimental data from Kundoor and Dalby.[30] This deposition region is caused by the high inertial droplet property and is caused by the inability of the nasal spray to fully expand within the confines of the nasal chamber. There are smaller local regions further downstream suggesting that a small fraction of droplets are able to penetrate the nasal valve region.

An additional important criterion for drug delivery efficiency is the deposition surface area or coverage, presented in the experimental work of Kundoor and Dalby.[30,33] However, quantifying this parameter by image analysis of three-dimensional models in two-dimensional images is difficult. An advantage of the computational simulation in this article is the ability to transform the three-dimensional bounding nasal cavity wall into a two-dimensional space. This is achieved by selecting a cut along the three-dimensional model that allows the surface to be unfurled and laid flat into a new two-dimensional plane, in what is called a *uv*-unwrapping method[32] (where *uv* represents the new transformed coordinates, *u* and *v*). Figure 9 shows the deposition pattern in the left nasal chamber on the *uv*-plane demonstrating the ability to quickly visualize the entire nasal cavity surface in one view. The deposition shows a concentration of deposited droplets in the vestibule across the roof and also on the inner septum wall region, while a small number of droplets enter the turbinate/meatus region.

Conclusion

The nozzle displacement during actuation, the spray plume development, and local averaged droplet size during the atomization process are sensitive to the actuation force applied on the atomizer. The nozzle displacement during actuation is characterized by two stages: the initial nozzle acceleration, and a steady displacement toward full displacement. The duration of each stage is shorter with increasing actuation pressure. Furthermore, the spray plume development during each stage was mapped, which showed different starting times for the spray plume expanding, being fully developed, and collapsing. The overall mean equivalent diameters were also determined where the droplet sizes were much smaller at the farthest radial distances than those found in the middle of the spray, a feature attributed to secondary breakup. The averaged local droplet velocity was also analyzed, and by using this known value along with the droplet size distribution, a CFD simulation using realistic boundary conditions was presented. The numerical results allowed visualization of the deposition pattern of spray droplets in the nasal cavity.

Acknowledgments

The authors gratefully acknowledge the financial support provided by the Australian Research Council (project ID: DP120103958).

Author Disclosure Statement

The authors declare that there are no conflicts of interest.

References

1. Dondeti P, Zia H, and Needham TE: In vivo evaluation of spray formulations of human insulin for nasal delivery. Int J Pharm. 1995;122:91–105.
2. Cheng YS, Holmes TD, Gao J, Guilmette RA, Li S, Surakitbanharn Y, and Rowlings C: Characterization of nasal spray pumps and deposition pattern in a replica of the human nasal airway. J Aerosol Med. 2001;14:267–280.
3. Suman JD, Laube BL, Lin TC, Brouet G, and Dalby R: Validity of in vitro tests on aqueous spray pumps as surrogates for nasal deposition. Pharm Res. 2002;19:1–6.
4. Dayal P, Shaik MS, and Singh M: Evaluation of different parameters that affect droplet-size distribution from nasal sprays using the Malvern Spraytec. J Pharm Sci. 2004;93:1725–1742.
5. Suman JD, Laube BL, and Dalby R: Validity of *in vitro* tests on aqueous spray pumps as surrogates for nasal deposition, absorption, and biologic response. J Aerosol Med. 2006;19:510–521.
6. Schroeter JD, Garcia GJM, and Kimbell JS: Effects of surface smoothness on inertial particle deposition in human nasal models. J Aerosol Sci. 2011;42:52–63.
7. Swift DL: Inspiratory inertial deposition of aerosols in human nasal airway replicate casts: implication for the proposed NCRP lung model. Radiat Prot Dosimetry. 1991;38:29–34.
8. Inthavong K, Tian ZF, Li HF, Tu JY, Yang W, Xue CL, and Li CG: A numerical study of spray particle deposition in a human nasal cavity. Aerosol Sci Technol. 2006;40:1034–1045.
9. Inthavong K, Tian ZF, Tu JY, Yang W, and Xue C: Optimising nasal spray parameters for efficient drug delivery using computational fluid dynamics. Comput Biol Med. 2008;38:713–726.
10. Inthavong K, Ge Q, Se CMK, Yang W, and Tu JY: Simulation of sprayed particle deposition in a human nasal cavity including a nasal spray device. J Aerosol Sci. 2011;42:100–113.
11. Foo M, Cheng Y, Su W, and Donovan M: The influence of spray properties on intranasal deposition. J Aerosol Med. 2007;20:495–508.

12. Vecellio L, De Gersem R, Le Guellec S, Reychler G, Pitance L, Le Pennec D, Diot P, Chantrel G, Bonfils P, and Jamar F: Deposition of aerosols delivered by nasal route with jet and mesh nebulizers. Int J Pharm. 2011;407:87–94.
13. Suman J, Laube B, and Dalby R: Comparison of nasal deposition and clearance of aerosol generated by a nebulizer and an aqueous spray pump. Pharm Res. 1999;16:1648–1652.
14. Kimbell JS, Segal RA, Asgharian B, Wong BA, Schroeter JD, Southall JP, Dickens CJ, Brace G, and Miller FJ: Characterization of deposition from nasal spray devices using a computational fluid dynamics model of the human nasal passages. J Aerosol Med. 2007;20:59–74.
15. Mitchell JP, Nagel MW, Nichols S, and Nerbrink O: Laser diffractometry as a technique for the rapid assessment of aerosol particle size from inhalers. J Aerosol Med. 2006;19:409–433.
16. Guo C, and Doub WH: The influence of actuation parameters on *in vitro* testing of nasal spray products. J Pharm Sci. 2006;95:2029–2040.
17. Guo C, Stine KJ, Kauffman JF, and Doub WH: Assessment of the influence factors on in vitro testing of nasal sprays using Box-Behnken experimental design. Eur J Pharm Sci. 2008;35:417–426.
18. Liu X, Doub WH, and Guo C: Evaluation of droplet velocity and size from nasal spray devices using phase Doppler anemometry (PDA). Int J Pharm. 2010;388:82–87.
19. Kippax PG, Krarup H, and Suman D: Applications for droplet sizing: manual versus automated actuation of nasal sprays. *Pharmaceutical Technology (Outsourcing Resources)*; pp. 30–39, August 2004.
20. Doughty DV, Vibbert C, Kewalramani A, Bollinger ME, and Dalby RN: Automated actuation of nasal spray products: determination and comparison of adult and pediatric settings. Drug Dev Ind Pharm. 2011;37:359–366.
21. Inthavong K, Yang W, Fung MC, and Tu JY: External and near-nozzle spray characteristics of a continuous spray atomized from a nasal spray device. Aerosol Sci Technol. 2012;46:165–177.
22. Fung MC, Inthavong K, Yang W, Lappas P, and Tu J: External characteristics of unsteady spray atomization from a nasal spray device. J Pharm Sci. 2013;102:1024–1035.
23. Yule AJ, Cox NW, and Chigier NA: Measurement of particle size in sprays by the automated analysis of spark photographs. In: *Particle Size Analysis*. Heyden, London; pp. 61–73, 1978.
24. Whybrew A, Nicholls TR, Boaler JJ, and Booth HJ: Diode lasers—a cost effective tool for simultaneous visualisation, sizing, and velocity measurements of sprays. In: *Proceedings of the 15th Annual Conference on Liquid Atomization and Spray Systems*. Toulouse, France, July 5–7, 1999.
25. Lefebvre AH: *Atomization and Sprays*. Hemisphere Publishing Corp., New York; 1989.
26. Fung MC, Inthavong K, Yang W, and Tu J: CFD modeling of spray atomization for a nasal spray device. Aerosol Sci Technol. 2012;46:1219–1226.
27. Wen J, Inthavong K, Tu JY, and Wang S: Numerical simulations for detailed airflow dynamics in a human nasal cavity. Respir Physiol Neurobiol. 2008;161:125–135.
28. Kelly JT, Asgharian B, Kimbell JS, and Wong BA: Particle deposition in human nasal airway replicas manufactured by different methods. Part 1: Inertial regime particles. Aerosol Sci Technol. 2004;38:1063–1071.
29. Shi H, Kleinstreuer C, and Zhang Z: Modeling of inertial particle transport and deposition in human nasal cavities with wall roughness. J Aerosol Sci. 2007;38:398–419.
30. Kundoor V, and Dalby RN: Effect of formulation- and administration-related variables on deposition pattern of nasal spray pumps evaluated using a nasal cast. Pharm Res. 2011;28:1895–1904.
31. Inthavong K, Tu J, and Heschl C: Micron particle deposition in the nasal cavity using the v2–f model. Comput Fluids. 2011;51:184–188.
32. Inthavong K, Shang Y, and Tu J: Surface mapping for visualization of wall stresses during inhalation in a human nasal cavity. Respir Physiol Neurobiol. 2014;190:54–61.
33. Kundoor V, and Dalby RN: Assessment of nasal spray deposition pattern in a silicone human nose model using a color-based method. Pharm Res. 2010;27:30–36.

Received on September 27, 2013
in final form, March 30, 2014

Reviewed by:
Yung-Sung Cheng
Daryl Roberts

Address correspondence to:
Dr. Jiyuan Tu
School of Aerospace, Mechanical and Manufacturing Engineering
RMIT University, PO Box 71
Bundoora, Victoria 3083
Australia

E-mail: jiyuan.tu@rmit.edu.au